Alternative mutational architectures can produce identical $\mathbf{M}$-matrices but lead to different macroevolutionary dynamics

Daohan Jiang[1] & Matt Pennell[1,2,*]

[1]*Department of Quantitative and Computational Biology, University of Southern California, USA*
[2]*Department of Biological Sciences, University of Southern California, USA*
[*]Corresponding author: mpennell@usc.edu

Abstract

Explaining macroevolutionary divergence in light of population genetics requires understanding the extent to which the patterns of mutational input contribute to long-term trends. In the context of quantitative traits, mutational input is typically described by the mutational variance-covariance matrix, or the $\mathbf{M}$-matrix, which summarizes phenotypic variances and covariances introduced by new mutations per generation. However, as a summary statistic, the $\mathbf{M}$-matrix does not fully capture the pleiotropic structure of the underlying mutational architecture, and there exist infinitely many possible underlying mutational architectures that give rise to the same $\mathbf{M}$-matrix. Here, using simulations, we demonstrate alternative mutational architectures underlying the same $\mathbf{M}$-matrix can lead to different levels of constraint on evolution and result in difference in rate and dynamics of adaptive evolution. We also found for a given $\mathbf{M}$-matrix, the evolutionary variance-covariance matrix, or the $\mathbf{R}$-matrix, is more strongly aligned to the $\mathbf{M}$-matrix when the underlying mutational architecture has stronger pleiotropy. Taken together, our results reveal that aspects of mutational input not reflected by the $\mathbf{M}$-matrix can have a profound impact on long-term evolution, and suggest it is important to take them into account in order to connect macroevolutionary patterns to microevolutionary mechanisms.

Article type: Short communication

Keywords: $\mathbf{M}$-matrix, macroevolutionary divergence, phenotypic evolution, pleiotropy

Introduction

A fundamental problem in evolutionary biology is explaining phenotypic diversity across species in light of population genetics [Arnold et al., 2001, Hansen and Houle, 2004, Harmon et al., 2021, Rolland et al., 2023] At least in some taxa, macroevolutionary divergence, captured by the variances and covariance in phenotypes among lineages on a phylogenetic tree, reflects the correlational structure of the additive genetic variance within lineages [Ackermann and Cheverud, 2004, Bolstad et al., 2014, McGlothlin et al., 2018, Opedal et al., 2023, Porto et al., 2015, Schluter, 1996]. While we expect the short term response to selection to be in the direction with the most additive genetic variance in the phenotypic space [Arnold, 1992, Lande, 1976, 1979, Walsh and Blows, 2009], it is intriguing that this appears to extend to longer term trends. Selection will tend to erode the additive genetic variance relatively quickly (at least relative to macroevolutionary timescales) so the structure of additive genetic variance must be maintained by some combination of drift, correlated selection, and correlated effects of mutations [Arnold, 1992, Arnold et al., 2008, Chakraborty and Nei, 1982, Cheverud, 1984, Jones et al., 2003, 2007, Lande, 1979, 1980, McGuigan, 2006, Svensson, 2022, Svensson et al., 2021]. For instance, strong alignment between the patterns genetic variation and macroevolutionary divergence either can be explained either by the absence of selection, or by a model where both are shaped by selection in the same way (i.e., traits or trait combinations subject to stronger selection have both lower genetic variances and lower evolutionary rates). The former explanation requires that the pattern of genetic variance reflects the patterns of mutational input — and this will be the focus of this paper.

That mutational structure is constraining the course of long-term phenotypic evolution is a long-standing and controversial hypothesis [Gould, 1980, Nei, 2013, Stoltzfus, 2021] but is notoriously difficult to test as the necessary data are very challenging to collect. A pioneering study [Houle et al., 2017] sought to take this on and test whether the observed correlations between the pattern of within-species additive genetic (co)variance (as encapsulated by the $\mathbf{G}$-matrix, hereafter $\mathbf{G}$) and the evolutionary phenotypic (co)variance (as encapsulated by the $\mathbf{R}$-matrix, hereafter $\mathbf{R}$) could be explained by mutations. Using wings of drosophilid flies as a model system, Houle et al. [2017] conducted laborious mutation accumulation (MA) experiments [reviewed in Halligan and Keightley, 2009] to estimate the mutational variance-covariance matrix (the $\mathbf{M}$-matrix, hereafter $\mathbf{M}$). The $\mathbf{M}$-matrix summarizes the amount and correlational structure of mutational input: each diagonal element of $\mathbf{M}$ represents a trait's mutational variance (i.e., phenotypic variance introduced by

new mutations per unit time, usually presented on a per-generation basis), and each off-diagonal element represents the mutational covariance (i.e., phenotypic covariance introduced by new mutations per generation) between two traits. They used genetic crosses to estimate $\mathbf{G}$ and collected phylogenetic data to estimate $\mathbf{R}$. They then tested whether $\mathbf{M}$, $\mathbf{G}$, and $\mathbf{R}$ were aligned — the level of similarity between the matrices can be evaluated by comparing variances in two matrices on a pre-specified set of orthogonal dimensions in the phenotypic space quantified by the correlation between the variances. Again, a positive result would be consistent with the patterns of mutational input driving long-term evolution, and this alignment is exactly what Houle et al. [2017] reported. However, the strength of the scaling relationship was likely mis-estimated [Jiang and Zhang, 2020] and it remains an open problem as to what the best estimate of the scaling relationship is and how best to interpret the estimate [Houle et al., 2020, Jiang and Zhang, 2020, Opedal et al., 2023]

Our purpose in this paper is not to delve into the analysis of this particular dataset; rather we will argue that the core predictions and interpretations of these tests — and future tests like them — are not as straightforward as they appear. The conceptual difficulty of testing for the role of mutation-drive macroevolution lies in the fact that $\mathbf{M}$ is an insufficient summary statistic for the mutational architecture. An important aspect of mutations that is not fully captured by $\mathbf{M}$ is the amount pleiotropy. Pleiotropy can constrain evolution because pleiotropic mutations are less likely to be beneficial and/or more likely to be deleterious [Barton, 1990, Chen and Zhang, 2020, Jiang and Zhang, 2020, Keightley and Hill, 1990, McGuigan et al., 2014, 2011, Orr, 2000, Turelli, 1985, Wagner, 1989, Welch and Waxman, 2003, Zhang and Hill, 2005]. On the other hand, an intermediate level of pleiotropy may also facilitate adaptation [Frachon et al., 2017, Rennison and Peichel, 2022, Wang et al., 2010]. But in either case, it is clearly important for understanding the evolvability of a phenotype [Hansen and Pélabon, 2021].

To see why $\mathbf{M}$ does not fully capture pleiotropy, consider two quantitative traits z_1 and z_2. Assuming only additive effects, there are three types of mutations: mutations that affect z_1 only, mutations that affect z_2 only, and pleiotropic mutations that affect both traits. Let us assume that the effect size of mutations that exclusively influence a single trait are drawn from normal distributions, $\mathcal{N}(0, \sigma_{e.1})$, and $\mathcal{N}(0, \sigma_{e.2})$, respectively, and the effect size of pleiotropic mutations follows a bivariate normal distribution characterized

by a covariance matrix:

$$\mathbf{M}_P = \begin{bmatrix} \sigma_{p.1}^2 & \rho\sigma_{p.1}\sigma_{p.2} \\ \rho\sigma_{p.1}\sigma_{p.2} & \sigma_{p.2}^2 \end{bmatrix}. \tag{1}$$

Here, $\sigma_{p.1}$ and $\sigma_{p.2}$ are the standard deviations of pleiotropic mutations' effects on z_1 and z_2, respectively, and ρ denotes the correlation between the mutations' effects on z_1 and their effects on z_2. The $\mathbf{M}$ matrix is obtained by combining the (co)variances resulting from pleiotropic and non-pleiotropic mutations:

$$\mathbf{M} = U_1 \begin{bmatrix} \sigma_{e.1}^2 & 0 \\ 0 & 0 \end{bmatrix} + U_2 \begin{bmatrix} 0 & 0 \\ 0 & \sigma_{e.2}^2 \end{bmatrix} + U_P \begin{bmatrix} \sigma_{p.1}^2 & \rho\sigma_{p.1}\sigma_{p.2} \\ \rho\sigma_{p.1}\sigma_{p.2} & \sigma_{p.2}^2 \end{bmatrix}$$

Here, U_1 represents the rate of mutations that affect z_1 only, U_2 represents the rate of mutations that affect z_2 only, and U_P represents the rate of pleiotropic mutations. Consequently, the first term in the equation represents mutational variance resulting from mutations that affect z_1 only, the second term represents mutational variance resulting from mutations that affect z_2 only, and the last term represents mutational (co)variances resulting from pleiotropic mutations. Adding up the tree terms in the previous equation gives:

$$\mathbf{M} = \begin{bmatrix} U_1\sigma_{e.1}^2 + U_P\sigma_{p.1}^2 & U_P\rho\sigma_{p.1}\sigma_{p.2} \\ U_P\rho\sigma_{p.1}\sigma_{p.2} & U_2\sigma_{e.2}^2 + U_P\sigma_{p.2}^2 \end{bmatrix} \tag{2}$$

We denote to a particular vector of values $\mathbb{P}$, where $\mathbb{P} : \{U_1, \sigma_{e.1}, U_2, \sigma_{e.2}, U_P, \rho, \sigma_{p.1}, \sigma_{p.2}\}$ hereafter for convenience. This model can be easily extended to phenotypic spaces with a higher number of dimensions; for an n-dimensional phenotypic space, the number of possible mutation types is equal to $\sum_{i=1}^{n} \binom{n}{i}$.

As shown in equation (2), each entry of $\mathbf{M}$ is contributed by multiple quantities. Thus, it is possible that different $\mathbb{P}$ give rise to the same $\mathbf{M}$ matrix. To see how we can manipulate the parameters while holding $\mathbf{M}$ constant, let U_P, ρ, $\sigma_{p.1}$, and $\sigma_{p.2}$ each be multiplied by a rescaling coefficient, such that they become $C_P U_P$, $C_\rho \rho$, $C_{p.1}\sigma_{p.1}$, and $C_{p.2}\sigma_{p.2}$, respectively, where $C_P C_\rho C_{p.1} C_{p.2} = 1$ and $C_\rho < 1/|\rho|$. Let us multiply $U_1\sigma_{e.1}^2$ and $U_2\sigma_{e.2}^2$ by rescaling coefficients C_1 and C_2, respectively, to keep the mutational variances unchanged:

$$\begin{cases} \mathbf{M}[1,1] = C_1 U_1 \sigma_{e.1}^2 + C_P C_{p.1}^2 U_P \sigma_{p.1}^2 & = U_1\sigma_{e.1}^2 + U_P\sigma_{p.1}^2 \\ \mathbf{M}[2,2] = C_2 U_2 \sigma_{e.1}^2 + C_P C_{p.2}^2 U_P \sigma_{p.2}^2 & = U_2\sigma_{e.2}^2 + U_P\sigma_{p.2}^2 \end{cases}$$

Solving the above equations gives

$$\begin{cases} C_1 = \dfrac{U_1\sigma_{e.1}^2 + (1 - C_P C_{p.1}^2)U_P\sigma_{p.1}^2}{U_1\sigma_{e.1}^2} \\ C_2 = \dfrac{U_2\sigma_{e.2}^2 + (1 - C_P C_{p.2}^2)U_P\sigma_{p.2}^2}{U_2\sigma_{e.2}^2} \end{cases} \tag{3}$$

C_1 and C_2 must be non-negative, as no mutation rate or standard deviation can be negative. Therefore, C_1 and C_2 can only be solved if

$$\begin{cases} U_1\sigma_{e.1}^2 + (1 - C_P C_{p.1}^2)U_P\sigma_{p.1}^2 > 0 \\ U_2\sigma_{e.2}^2 + (1 - C_P C_{p.2}^2)U_P\sigma_{p.2}^2 > 0 \end{cases}$$

Solving the above system of inequities gives

$$\begin{cases} C_P C_{p.1}^2 < \dfrac{U_1\sigma_{e.1}^2}{U_P\sigma_{p.1}^2} + 1 \\ C_P C_{p.2} b^2 < \dfrac{U_2\sigma_{e.2}^2}{U_P\sigma_{p.2}^2} + 1 \end{cases} \tag{4}$$

Hence, given $\mathbf{M}$, certain combinations of C_P, C_ρ, $C_{p.1}$, and $C_{p.2}$ are guaranteed to alter the mutational variances. Biologically, if the portion of mutational variance attributable to pleiotropic mutations gets too high, it would be impossible to keep the total mutational variance unchanged by reducing the portion contributed by non-pleiotropic mutations.

Given that C_1 can be solved, the change to $U_1\sigma_{e.1}^2$ can be done by altering U_1, $\sigma_{e.1}$, or both. Thus, for any given combination of C_P, C_ρ, $C_{p.1}$, and $C_{p.2}$, there exists infinitely many ways to adjust $U_1\sigma_{e.1}^2$ to keep $\mathbf{M}$ unchanged. Similarly, there are also infinitely many ways to adjust $U_2\sigma_{e.2}^2$. Hence, there exists infinitely many unique $\mathbb{P}$ that give rise to the same $\mathbf{M}$ matrix.

In this study, we use simulations to illustrate that the long-term evolutionary trajectory of a population depends not just on $\mathbf{M}$ but on the underlying structure of pleiotropy. Since there is a many-to-one mapping between $\mathbb{P}$ and $\mathbf{M}$, one cannot make clear predictions as to the expected relationship between $\mathbf{M}$, $\mathbf{G}$, and $\mathbf{R}$ without additional information or assumptions.

Materials and Methods

Generating series of mutational parameter combinations giving rise to the same M matrix

We considered two properties of the mutational architecture that could potentially affect the extent to which evolution is constrained by pleiotropy. First, we looked at the deleteriousness of pleiotropic mutations — how deleterious a pleiotropic mutation is determined by the distribution of effect size of pleiotropic mutations; Second, we looked at the proportion of mutational variance attributable to pleiotropic mutations. To demonstrate how these properties of the mutational architecture could lead to different outcomes in long-term evolution, we considered two $\mathbf{M}$-matrices as examples, including a matrix with zero mutational covariance and one with a positive mutational covariance. For each example matrix, we started from a set of mutational parameters $\mathbb{P}$ and then applied a transformation to obtain a set of parameters $\mathbb{P}'$ that maintained all entries of $\mathbf{M}$, with the effect size distribution or mutational variances caused by pleiotropic mutations altered. We then compared the evolutionary dynamics when assuming $\mathbb{P}$ versus assuming $\mathbb{P}'$.

To adjust the distribution of effect sizes of pleiotropic mutations, we adjusted U_P, $\sigma_{p.1}$, and $\sigma_{p.2}$ and let changes in these three parameters cancel out to keep the mutational covariance unchanged. Let U_P become CU_P, $\sigma_{p.1}$ become $\sqrt{C}\sigma_{p.1}$, and $\sigma_{p.2}$ become $\sqrt{C}\sigma_{p.2}$, respectively, such that the mutational covariance remains unchanged:

$$\mathbf{M}[1,2] = \mathbf{M}[2,1] = (CU_P)\rho(\sqrt{C}\sigma_{p.1})(\sqrt{C}\sigma_{p.2}) = U_P\rho\sigma_{p.1}\sigma_{p.2}$$

Diagonal elements of $\mathbf{M}$ remain unchanged while no other parameters are altered:

$$\begin{cases} \mathbf{M}[1,1] = U_1\sigma_{e.1}^2 + (CU_P)(C\sigma_{p.1}^2) = U_1\sigma_{e.1}^2 + U_P\sigma_{p.1}^2 \\ \mathbf{M}[2,2] = U_2\sigma_{e.1}^2 + (CU_P)(C\sigma_{p.2}^2) = U_2\sigma_{e.2}^2 + U_P\sigma_{p.2}^2 \end{cases}$$

In this case, the proportion of mutational variance resulting from pleiotropic mutations remains constant for both traits, while the distribution of phenotypic effect of pleiotropic mutations changed.

To adjust the proportion of mutational variance attributable to pleiotropic mutations while keeping the $\mathbf{M}$ matrix unchanged, we changed ρ and U_P with the mutational covariance held unchanged and then altered

U_1 and U_2 accordingly to keep the mutational variances the same using the following procedure. Let U_P become CU_P and ρ become $C^{-1}\rho$, where $C > |\rho|$, such that:

$$\mathbf{M}[1,2] = \mathbf{M}[2,1] = (CU_P)(C^{-1}\rho)\sigma_{p.1}\sigma_{p.2} = U_P\rho\sigma_{p.1}\sigma_{p.2}$$

Let us then multiply $U_1\sigma_{e.1}^2$ and $U_2\sigma_{e.2}^2$ by C_1 and C_2, respectively, to keep diagonal elements of $\mathbf{M}$ unchanged. C_1 and C_2 can be obtained using (3):

$$\begin{cases} C_1 = \dfrac{U_1\sigma_{e.1}^2 + (1-C)U_P\sigma_{p.1}^2}{U_1\sigma_{e.1}^2} \\ C_2 = \dfrac{U_2\sigma_{e.2}^2 + (1-C)U_P\sigma_{p.2}^2}{U_2\sigma_{e.2}^2} \end{cases}$$

In this case, the distribution of pleiotropic mutations' effect on individual traits remains unchanged as $\sigma_{p.1}$ and $\sigma_{p.2}$ are unchanged, but the relative contribution of pleiotropic mutations to each traits mutational variance changed.

The first example $\mathbf{M}$ we examined has zero covariance:

$$\mathbf{M} = \begin{bmatrix} 0.01 & 0 \\ 0 & 0.01 \end{bmatrix}$$

For this example $\mathbf{M}$, we started from $\mathbb{P} : \{U_1 = U_2 = U_P = 1, \sigma_{e.1} = \sigma_{e.2} = \sigma_{p.1} = \sigma_{p.2} = 0.1\}$. When adjusting the distribution of effect sizes of pleiotropic mutations, we chose values of C such that U_P would be multiplied by 10^{-4}, 10^{-3}, 10^{-2}, 10^{-1}, 10, 10^2, 10^3, and 10^4 (Table S1, rows 1-9). When adjusting the proportion of mutational variances contributed by pleiotropic mutations, values of C were chosen such that the proportion would take 0%, 10%, 20%, ..., 100% (Table S1, rows 10-19).

The other $\mathbf{M}$ examined here has a positive covariance:

$$\mathbf{M} = \begin{bmatrix} 0.01 & 0.005 \\ 0.005 & 0.01 \end{bmatrix}$$

For this example, $\mathbb{P} : \{U_1 = U_2 = U_P = 1, \sigma_{e.1} = \sigma_{e.2} = \sigma_{p.1} = \sigma_{p.2} = 0.1, \rho = 0.5\}$. When

adjusting the distribution of effect sizes of pleiotropic mutations, values of C were chosen such that U_P would be multiplied by 10^{-4}, 10^{-3}, 10^{-2}, 10^{-1}, 10, 10^2, 10^3, and 10^4 (Table S2, rows 1-9), as we did in the case of zero mutational covariance. When adjusting the proportion of mutational variance contributed by pleiotropic mutations, values of C were chosen such that ρ would take 0.3, 0.4, 0.6, 0.7, 0.8, and 0.9 (Table S2, rows 11-15).

Mapping between phenotype and fitness

We considered a multivariate Gaussian fitness function, which is described by a covariance matrix $\mathbf{S}$. Each diagonal element of $\mathbf{S}$ is the variance of an individual trait's fitness function, and off-diagonal elements represent correlational selection for allometric relationships between traits [Arnold et al., 2008, 2001]. Because we only considered two traits in this study, the $\mathbf{S}$ matrix can be written simply as

$$\mathbf{S} = \begin{bmatrix} s_1^2 & s_1 s_2 \rho_s \\ s_1 s_2 \rho_s & s_2^2 \end{bmatrix} \tag{5}$$

In the above matrix, s_1 and s_2 are standard deviations of fitness functions of two individual traits. Correlational selection is characterized by the correlation coefficient ρ_s.

To calculate fitness given the bivariate phenotype $\vec{z} = (z_1, z_2)$, we first calculate its distance to the optimal phenotype $\vec{o}$:

$$\vec{d} = \vec{z} - \vec{o} = (z_1 - o_1, z_2 - o_2)$$

We then calculate the projection of $\vec{d}$ on eigenvectors of $\mathbf{S}$:

$$\vec{b} = \vec{d}\mathbf{H}$$

Here, $\mathbf{H}$ is the eigenvector matrix of $\mathbf{S}$. The fitness is then calculated as

$$\omega = \exp\left(-\left(\frac{{b_1}^2}{2E_1} + \frac{{b_2}^2}{2E_2}\right)\right) \tag{6}$$

Here, b_1 and b_2 are the two elements of $\vec{b}$, while E_1 and E_2 are the first and second eigenvalues of $\mathbf{S}$, respectively. If an eigenvalue of $\mathbf{S}$ (e.g., E_i) is non-positive, the corresponding term in (6) ($\frac{{b_i}^2}{2E_i}$) would be dropped.

The biological interpretation of such a situation is the lack of selection on a specific phenotypic dimension, in which case the phenotypic dimension with no selection should not be considered when calculating fitness.

Simulation of evolution

For each $\mathbb{P}$ and regime of selection, we simulated a number of replicate lineages and tracked each lineage's population mean phenotypes through time. We simulated 500 replicate lineages for each combination of parameters (i.e., $\mathbb{P}$ and $\mathbf{S}$), and the phenotype at the beginning was set at $(0, 0)$ for all simulations.

For the $\mathbf{M}$ matrix with zero covariance, we simulated evolution under the following two scenarios:

SC1: In this scenario both traits are under consideration are under stabilizing selection and there is no correlational selection. The optimal phenotype is set to be $(0, 0)$, and the $\mathbf{S}$ matrix is:

$$\mathbf{S} = \begin{bmatrix} 5 & 0 \\ 0 & 5 \end{bmatrix}$$

For this scenario, we specifically examined the variance among replicate lineages at the end of the simulations, which represent the amount of evolutionary divergence accumulated through time. We calculated the standard deviation of this sample variance as

$$\mathrm{SD}(\mathcal{V}) = \sqrt{\frac{2\hat{\mathcal{V}}^2}{n-1}}$$

In the above formula, $\hat{\mathcal{V}}$ is the observed variance of a trait among lineages and n is the number of lineages.

SC2: One trait is under directional selection, and the other is under directional selection. The optimal phenotype is set to be $(10, 0)$, and the $\mathbf{S}$ matrix is

$$\mathbf{S} = \begin{bmatrix} 1 & 0 \\ 0 & 1 \end{bmatrix}$$

We had the strength of selection stronger than that in SC1 to better demonstrate the effect of constraint.

For the $\mathbf{M}$ with a positive covariance, we additionally simulated evolution under the following scenarios:

sc3: The optimal phenotype is set to be $(10, -10)$, and the $\mathbf{S}$ matrix is the same as that in sc2:

$$\mathbf{S} = \begin{bmatrix} 1 & 0 \\ 0 & 1 \end{bmatrix}$$

In the scenario, direction of selection (i.e., the line connecting the ancestral phenotype and the optimum) is orthogonal to the the first eigenvector of the $\mathbf{M}$ matrix.

sc4: The optimal phenotype is set to be $(10, -10)$, and the $\mathbf{S}$ matrix is

$$\mathbf{S} = \begin{bmatrix} 1 & -0.9 \\ -0.9 & 1 \end{bmatrix}$$

The covariance of the $\mathbf{S}$ matrix means correlational selection is present. In this scenario, both the direction of selection and the first eigenvector of $\mathbf{S}$ are orthogonal to the first eigenvector of $\mathbf{M}$. This scenario is similar to that considered when conditional evolvability is evaluated – directional selection is acting on a specific combination of traits while other combinations are subject to stabilizing selection [Hansen and Houle, 2008, Hansen et al., 2019].

For all scenarios with directional selection, we quantified the rate of adaptation for each lineage by averaging its fitness at all time steps, which we refer to as the lineage's integrated fitness of lineage. The integrated fitness of lineage i is calculated as

$$\bar{\omega}_i = \frac{1}{T} \sum_{t=0}^{T} \omega_{i,t} \tag{7}$$

Here, T is the total number of time steps, and $\omega_{i,t}$ is the fitness of lineage i at time t. If adaptation is fast such that the optimum is quickly reached, most fitness values would be close to the maximum, and $\bar{\omega}_i$ would be high; if adaptation is slow, there would be more low fitness values in the series, resulting in lower $\bar{\omega}_i$. For each $\mathbb{P}$, we averaged all replicate lineages' integrated fitness to estimate the average rate of adaptation for this

parameter combination.

$$\bar{\omega} = \frac{1}{n}\sum_{i=0}^{n}\bar{\omega}_i \tag{8}$$

Here, n is the number of replicate lineages.

Simulation along each replicate lineage followed a sequential fixation model. Simulations of evolution under stabilizing selection lasted 2×10^4 time steps for each lineage, whereas simulations of evolution under stabilizing selection lasted 2×10^3 time steps for each lineage. In each time step, we first determined the number of mutations that would occur, n_t, which was sampled from a Poisson distribution with mean equal to $U_1 + U_2 + U_3$. The probability that a mutation affects z_1 only is $\frac{U_1}{U_1+U_2+U_3}$, the probability it affects z_2 only is $\frac{U_2}{U_1+U_2+U_3}$, and the probability it is pleiotropic is $\frac{U_P}{U_1+U_2+U_3}$. If the mutation affects z_1 only, its effect size would be sampled from a normal distribution $\mathcal{N}(0, \sigma_{e.1})$. Similarly, if it affects z_2 only, its effect size would be sampled from $\mathcal{N}(0, \sigma_{e.2})$. If it is pleiotropic, its effect would be sampled from a bivariate normal distribution described by a matrix $\mathbf{M}_P$, as described in equation (1).

After determining the mutation's phenotypic effect, the mutant's fitness was calculated following (6). The coefficient of selection was calculated as $s = \omega/\omega_A - 1$, where ω and ω_A are mutant and ancestral fitness, respectively. Given the effective population size N_e, fixation probability of the mutation is calculated as following Kimura's method [Kimura, 1962]:

$$p_f = \frac{1 - \exp(-2s)}{1 - \exp(-4N_e s)} \tag{9}$$

With probability p_f, phenotypic effect of the mutation would be added to the population's mean phenotype before the next mutation is considered. We had effective population size $N_e = 10^3$ for all simulations.

Alignment between high-dimensional $\mathbf{M}$ and $\mathbf{R}$ matrices

In addition to the simple case of two traits described above, we also considered a 10-dimensional phenotypic space and conducted simulations of evolution of the ten traits. The mutational variance-covariance matrix considered here, $\mathbf{M}_{10}$, is a 10×10 diagonal matrix with elements equal to $\exp(-9)$, $\exp(-8)$, $\exp(-7)$, $\ldots$, $\exp(0)$. As the number of mutation parameters is large (1024 in total), we only considered two extreme cases: a mutational architecture characterized by a lack of pleiotropy (i.e., every mutation affects one trait only),

and one characterized by universal pleiotropy (i.e., every mutation affects all traits). In the first case, there are ten types of mutations (mutations affecting $z_1, \ldots,$ mutations affecting z_{10}) and 20 underlying parameters ($U_1, \ldots, U_{10}, \sigma_{e.1}, \ldots, \sigma_{10}$). In our simulations, we had $U_1 = \ldots = U_{10} = 1$ and $\sigma^2_{e.1} = \mathbf{M}_{10}[1,1], \ldots,$ $\sigma^2_{10} = \mathbf{M}_{10}[10,10]$. In the case of universal pleiotropy, there is only one type of mutation, of which the rate was set to be 1, and the effect of mutation on traits follows a multivariate normal distribution corresponding to $\mathbf{M}_{10}$.

For this 10-dimensional phenotypic space, we simulated evolution under stabilizing selection for 500 lineages and had the simulation last for $T = 5 \times 10^4$ time steps for each lineage. The optimal phenotype is 0 for all dimensions, which is also the starting state of all lineages. The matrix of selection $\mathbf{S}$ is a diagonal matrix with every diagonal element equal to 10, such that there is no correlational selection and the strength of selection is the same for all traits.

After the simulations, we calculated the evolutionary variance-covariance matrix ($\mathbf{R}$) and compared its diagonal elements (i.e., the $\mathbf{R}$ variances) to those of $\mathbf{M}$ (i.e., the $\mathbf{M}$ variances). Similarity between $\mathbf{M}$ and $\mathbf{R}$ is measured by Pearson's correlation coefficient between natural logarithms of the $\mathbf{M}$ variances and those of the $\mathbf{R}$ variances, as well as the linear regression slope of the $\mathbf{R}$ variances' natural logarithms on the $\mathbf{M}$ variances' natural logarithms. For each trait, we calculated Pearson's correlation coefficient between the amount of variance across lineages and time as a measurement of phylogenetic signal. All simulations and analyses were done in R.

Results

Different mutational architecture of the same $\mathbf{M}$-matrix constrain adaptation differently

We found the rate of adaptation varied greatly among combinations of mutational parameters that give rise to the same $\mathbf{M}$-matrix but vary in terms of the effect size distribution of pleiotropic mutations. Specifically, the mean integrated fitness became higher when the rate of pleiotropic mutations become higher (i.e., higher U_P) but their phenotypic effects became weaker (i.e., smaller $\sigma_{p.1}$ and $\sigma_{p.2}$), which is true for both the $\mathbf{M}$ matrix with zero covariance (Fig. 1A) and the one with a positive covariance (Fig. 2A, C, and E), and for all three selective regimes with directional selection (sc2, sc3, and sc4).

Various $\mathbb{P}$ that vary in terms of the contribution of pleiotropic mutations to mutational variances, in contrast, did not vary as much in terms of integrated fitness in scenarios (Fig. 1B, Fig. 2B and D), which is not too unexpected became the U_P could only vary in a relatively small range in this case. However, in scenario sc3, where correlational selection was present, the integrated fitness decreased as the strength of correlation between pleiotropic mutations' effects on two traits (ρ) increased (Fig. 2F). In other words, constraint on adaptation became stronger when pleiotropic mutations are more deleterious and less likely to be beneficial due to worse alignment between pleiotropic mutations' phenotypic effects and the fitness ridge (i.e., the first eigenvector of $\mathbf{S}$).

We also simulated evolution of the two traits under stabilizing selection with the same $\mathbb{P}$. We examined how the amount of evolutionary divergence (i.e., phenotypic variance) among lineages varied with changes to $\mathbb{P}$, but found little difference among mutational parameter combinations in either the case of zero mutational covariance (Fig. S1) or the case of non-zero covariance (Fig. S2).

Alignment between $\mathbf{M}$ and $\mathbf{R}$ enhanced by pleiotropy

When pleiotropy is absent, the then traits had rather similar $\mathbf{R}$ variances, and the $\mathbf{R}$ variances are not significantly correlated with the $\mathbf{M}$ variances (Fig. 3A), indicating the rate of evolutionary divergence is mainly determined by strength of selection rather than mutational input. In the presence of universal pleiotropy, $\mathbf{R}$ variances of many traits become much lower than in the absence of pleiotropy (from $\approx 30\%$ to $\approx 1\%$ of the corresponding $\mathbf{R}$ variances without pleiotropy, Fig. 3B), demonstrating constraint imposed by pleiotropy. Interestingly, $\mathbf{R}$ variances are strongly correlated to $\mathbf{M}$ ($r > 0.9$ between log-transformed variances, Fig. 3B). The least-squares regression line of log-transformed $\mathbf{R}$ variance on log-transformed $\mathbf{M}$ variance has a slope < 1 (Fig. 3B), which means the relationship between $\mathbf{M}$ and $\mathbf{R}$ variances are non-linear, and traits with greater $\mathbf{M}$ variance are affected more by constraint resulting from pleiotropy. In addition, when we examined phylogenetic signal of each trait, which is represented by the correlation between time and phenotypic variance among lineages, we found all traits exhibited stronger phylogenetic signal in the presence of pleiotropy (Table S3).

Discussion

In this study, we show a many-to-one mapping from the mutational architecture to the mutational variance-covariance matrix $\mathbf{M}$ and how alternative mutational architectures that map to the same $\mathbf{M}$ can lead to different evolutionary dynamics over long time scales. Using simulations, we show the distribution of effect sizes of pleiotropic mutations can have an appreciable impact on dynamics of adaptive evolution for given the $\mathbf{M}$ matrix. The same mutational covariances can result from a relatively small number of pleiotropic mutations with large phenotypic effects (i.e., low U_P but large $\sigma_{p.1}$ and $\sigma_{p.2}$), or a greater number of pleiotropic mutations with small phenotypic effects (i.e., high U_P but small $\sigma_{p.1}$ and $\sigma_{p.2}$), and in the former case, pleiotropic mutations are less likely to contribute to adaptation, resulting in a lower rate of adaptation (Fig. 1A, Fig. 2A, C, and E), presumably because pleiotropic mutations with large effect sizes are more likely to have a deleterious effect [Fisher, 1930, Orr, 2000].

The same mutational covariance can also result from different combinations of the rate of pleiotropic mutations (U_P) and the correlation between the pleiotropic mutations' effects on different traits ($|\rho|$). When correlational selection is present, this difference can have a profound impact on adaptation. If the first eigenvector of $\mathbf{M}$ matrix is poorly align with that of the adaptive landscape, a greater $|\rho|$ makes pleiotropic mutations more likely to be deleterious and less likely to be involved in adaptation, ultimately leading to slower adaptation (Fig. 2F).

Importantly and most relevant to the previous tests of mutation driven evolution by [Houle et al., 2017, Jiang and Zhang, 2020], the underlying architecture is the alignment between the $\mathbf{M}$ matrix and the $\mathbf{R}$ matrix. By simulating evolution in a 10-dimensional phenotypic space, we show the alignment between $\mathbf{M}$ and $\mathbf{R}$ is much stronger when there is universal pleiotropy but no correlation between mutations' effects on different traits compared to that in the absence of pleiotropy. It is worth noting the our observation is similar to patterns previously observed in wing morphology traits in drosophilid flies in terms of evolutionary rates, phylogenetic signal, and the regression slope of $\mathbf{R}$ variances on $\mathbf{M}$ variances after methodological bias is accounted for [Houle et al., 2017, Jiang and Zhang, 2020], suggesting constraint resulting from widespread pleiotropy is a plausible explanation for these observations.

Consequently, in order to make sense of any correlation between $\mathbf{M}$ and $\mathbf{R}$, one must also make some strong assumptions about the nature of pleiotropy. Models for the evolution of multivariate traits often assume

universal pleiotropy, where every mutation affects every phenotype. For instance, Fisher's Geometric Model makes this assumption, which leads to the prediction that mutations with smaller effect sizes are more likely to be adaptive and that there is a "cost of complexity" as adaptation is slower when there is a greater number of phenotypic dimensions [Fisher, 1930, Orr, 2000, Tenaillon, 2014, Welch and Waxman, 2003]. Similarly, in a series of modeling studies, Jones et al. [2007] and Jones et al. [2014] assumed universal pleiotropy when modeling the evolution of the mutational architecture under second-order selection, with the effect size correlation ρ being the the evolvable aspect of pleiotropy; if the assumption of universal pleiotropy is relaxed, other parameters (e.g., U_P) may respond to the same selection instead, and ρ may not respond as much to selection as predicted. The degree to which such assumptions are reasonable remains an open question in quantitative genetics [Boyle et al., 2017, Hill and Zhang, 2012a,b, Paaby and Rockman, 2013, Wagner and Zhang, 2011]. Some studies have found that each gene or mutation typically affects only a small subset of traits [Ho and Zhang, 2014, Wagner et al., 2008, Wang et al., 2010]. Others argue that pleiotropy is more pervasive and that many empirical studies underestimate the prevalence of pleiotropy due to technical issues Hill and Zhang [2012b]. Proponents of the recently proposed "omnigenic" model argue the weight of evidence from genetic mapping studies (particularly in the context of human diseases) indicate that each mutation can affect a large number of traits because of properties of the regulatory network [Boyle et al., 2017, Liu et al., 2019]. One way to make sense of these mixed results is to conclude that it is likely each individual gene or mutation usually has major effect on only a small set of traits, but may have small effects on many more traits — in other words, pleiotropy is widespread but the distribution of effect sizes is highly skewed. In any case, resolving this long-standing debate is well outside the scope of the current paper.

We have discussed how pleiotropy is not fully captured by various summaries (e.g., $\mathbf{M}$, $\mathbf{G}$) in the context of tests of mutation-driven macroevolution but the underlying principle likely clouds the interpretation of other tests. For example, researchers have hypothesized that the underlying genetic architecture of multivariate traits can evolve to be modular such that mutations tend not to affect traits belong to different functional modules simultaneously; this leads to enhanced evolvability and/or mutational robustness [De Visser et al., 2003, Goswami et al., 2014, Melo and Marroig, 2015, Wagner, 1996, Wagner and Altenberg, 1996, Wagner et al., 2007, Wagner and Zhang, 2011]. A widely used method to quantify modularity is the covariance ratio, a statistic that summarizes the overall amount of covariance between traits of different pre-defined modules relative to the overall amount of within-module covariance [Adams, 2016, Adams and Collyer, 2019]. How-

ever, as covariances do not fully capture properties of pleiotropic mutations, tests based on the covariance ratio may not capture modularity of the genotype-phenotype map. For example, if pleiotropy is indeed restricted within functional modules, yet mutations' effects on traits are not well correlated, there may not be signal of modularity in covariance-based tests, despite such a scenario shall still be considered a case of modularity. Thus, a comprehensive picture of mutations' effects on traits is essential for our understanding of modularity but investigating this point is beyond the scope of the present paper.

Furthermore, for the purpose of study, we focused on many-to-one mapping between underlying mutational architectures and the $\mathbf{M}$ matrix due to variation in rates and distributions of effect sizes of different classes of mutations. In addition to these aspects of the mutational architecture, there are others that are also not captured by mutational (co)variances yet can potentially affect the pattern of evolutionary divergence at least under some conditions, such as normality of the distribution of phenotypic effects of mutations [Schraiber and Landis, 2015], the number of loci underlying the trait [Lynch, 2020, Lynch and Hagner, 2015, Schraiber and Landis, 2015], and mutational bias [Svensson and Berger, 2019]. We would encourage theorists and empiricists to pay close attention to the (often implicit) assumptions about underlying architecture of traits embedded in both models and statistical tests.

Conclusions

Our results demonstrate that the $\mathbf{M}$-matrix, a summary statistic commonly used to describe mutational input for quantitative traits, does not fully capture key features of the mutational architecture even when mutations' effects are all additive. We show different mutational architectures that give rise to the same $\mathbf{M}$ can lead to different evolutionary dynamics. In particular, different properties of these mutational architectures can result in difference in the rate of adaptive evolution and alignment between patterns of mutational input and that of macroevolutionary divergence. Specifically, if a given $\mathbf{M}$ emerges from a model with high-levels of pleiotropy we expect a tighter alignment between $\mathbf{M}$ and $\mathbf{R}$ than if the same $\mathbf{M}$ emerged from a model with less pleiotropy. We suggest the many-to-one mapping between the underlying mutational architectures and the $\mathbf{M}$ matrix may contribute to the challenge of explaining macroevolutionary divergence in light of population-level measures.

Code availability

All R code to reproduce our results are available on GitHub (`https://github.com/phylo-lab-usc/m-matrix/`).

Acknowledgements

We thank Josh Schraiber and Alex Cope for thoughtful comments on the ideas in this paper. M.P. was supported by startup funds from the University of Southern California.

References

Ackermann, R. R. and J. M. Cheverud. 2004. Detecting genetic drift versus selection in human evolution. Proceedings of the National Academy of Sciences 101:17946–17951.

Adams, D. C. 2016. Evaluating modularity in morphometric data: challenges with the rv coefficient and a new test measure. Methods in Ecology and Evolution 7:565–572.

Adams, D. C. and M. L. Collyer. 2019. Comparing the strength of modular signal, and evaluating alternative modular hypotheses, using covariance ratio effect sizes with morphometric data. Evolution 73:2352–2367.

Arnold, S. J. 1992. Constraints on phenotypic evolution. The American Naturalist 140:S85–S107.

Arnold, S. J., R. Bürger, P. A. Hohenlohe, B. C. Ajie, and A. G. Jones. 2008. Understanding the evolution and stability of the g-matrix. Evolution 62:2451–2461.

Arnold, S. J., M. E. Pfrender, and A. G. Jones. 2001. The adaptive landscape as a conceptual bridge between micro-and macroevolution. Microevolution rate, pattern, process Pages 9–32.

Barton, N. H. 1990. Pleiotropic models of quantitative variation. Genetics 124:773–782.

Bolstad, G. H., T. F. Hansen, C. Pélabon, M. Falahati-Anbaran, R. Pérez-Barrales, and W. S. Armbruster. 2014. Genetic constraints predict evolutionary divergence in dalechampia blossoms. Philosophical Transactions of the Royal Society B: Biological Sciences 369:20130255.

Boyle, E. A., Y. I. Li, and J. K. Pritchard. 2017. An expanded view of complex traits: from polygenic to omnigenic. Cell 169:1177–1186.

Chakraborty, R. and M. Nei. 1982. Genetic differentiation of quantitative characters between populations or species: I. mutation and random genetic drift. Genetics Research 39:303–314.

Chen, P. and J. Zhang. 2020. Antagonistic pleiotropy conceals molecular adaptations in changing environments. Nature ecology & evolution 4:461–469.

Cheverud, J. M. 1984. Quantitative genetics and developmental constraints on evolution by selection. Journal of theoretical biology 110:155–171.

De Visser, J. A. G., J. Hermisson, G. P. Wagner, L. A. Meyers, H. Bagheri-Chaichian, J. L. Blanchard, L. Chao, J. M. Cheverud, S. F. Elena, W. Fontana, et al. 2003. Perspective: evolution and detection of genetic robustness. Evolution 57:1959–1972.

Fisher, R. A. 1930. The genetical theory of natural selection. The Clarendon Press.

Frachon, L., C. Libourel, R. Villoutreix, S. Carrère, C. Glorieux, C. Huard-Chauveau, M. Navascués, L. Gay, R. Vitalis, E. Baron, et al. 2017. Intermediate degrees of synergistic pleiotropy drive adaptive evolution in ecological time. Nature ecology & evolution 1:1551–1561.

Goswami, A., J. B. Smaers, C. Soligo, and P. D. Polly. 2014. The macroevolutionary consequences of phenotypic integration: from development to deep time. Philosophical Transactions of the Royal Society B: Biological Sciences 369:20130254.

Gould, S. J. 1980. Is a new and general theory of evolution emerging? Paleobiology 6:119–130.

Halligan, D. L. and P. D. Keightley. 2009. Spontaneous mutation accumulation studies in evolutionary genetics. Annual Review of Ecology, Evolution, and Systematics 40:151–172.

Hansen, T. F. and D. Houle. 2004. Evolvability, stabilizing selection, and the problem. Phenotypic integration: Studying the ecology and evolution of complex phenotypes Page 130.

Hansen, T. F. and D. Houle. 2008. Measuring and comparing evolvability and constraint in multivariate characters. Journal of evolutionary biology 21:1201–1219.

Hansen, T. F. and C. Pélabon. 2021. Evolvability: a quantitative-genetics perspective. Annual Review of Ecology, Evolution, and Systematics 52:153–175.

Hansen, T. F., T. M. Solvin, and M. Pavlicev. 2019. Predicting evolutionary potential: a numerical test of evolvability measures. Evolution 73:689–703.

Harmon, L. J., M. W. Pennell, L. F. Henao-Diaz, J. Rolland, B. N. Sipley, and J. C. Uyeda. 2021. Causes and consequences of apparent timescaling across all estimated evolutionary rates. Annual Review of Ecology, Evolution, and Systematics 52:587–609.

Hill, W. G. and X.-S. Zhang. 2012a. Assessing pleiotropy and its evolutionary consequences: pleiotropy is not necessarily limited, nor need it hinder the evolution of complexity. Nature Reviews Genetics 13:296–296.

Hill, W. G. and X.-S. Zhang. 2012b. On the pleiotropic structure of the genotype–phenotype map and the evolvability of complex organisms. Genetics 190:1131–1137.

Ho, W.-C. and J. Zhang. 2014. The genotype–phenotype map of yeast complex traits: basic parameters and the role of natural selection. Molecular biology and evolution 31:1568–1580.

Houle, D., G. H. Bolstad, and T. F. Hansen. 2020. Fly wing evolutionary rate is a near-isometric function of mutational variation. bioRxiv Pages 2020–08.

Houle, D., G. H. Bolstad, K. van der Linde, and T. F. Hansen. 2017. Mutation predicts 40 million years of fly wing evolution. Nature 548:447–450.

Jiang, D. and J. Zhang. 2020. Fly wing evolution explained by a neutral model with mutational pleiotropy. Evolution 74:2158–2167.

Jones, A. G., S. J. Arnold, and R. Bürger. 2003. Stability of the g-matrix in a population experiencing pleiotropic mutation, stabilizing selection, and genetic drift. Evolution 57:1747–1760.

Jones, A. G., S. J. Arnold, and R. Bürger. 2007. The mutation matrix and the evolution of evolvability. Evolution 61:727–745.

Jones, A. G., R. Bürger, and S. J. Arnold. 2014. Epistasis and natural selection shape the mutational architecture of complex traits. Nature communications 5:3709.

Keightley, P. D. and W. G. Hill. 1990. Variation maintained in quantitative traits with mutation–selection balance: pleiotropic side-effects on fitness traits. Proceedings of the Royal Society of London. Series B: Biological Sciences 242:95–100.

Kimura, M. 1962. On the probability of fixation of mutant genes in a population. Genetics 47:713.

Lande, R. 1976. Natural selection and random genetic drift in phenotypic evolution. Evolution Pages 314–334.

Lande, R. 1979. Quantitative genetic analysis of multivariate evolution, applied to brain: body size allometry. Evolution Pages 402–416.

Lande, R. 1980. The genetic covariance between characters maintained by pleiotropic mutations. Genetics 94:203–215.

Liu, X., Y. I. Li, and J. K. Pritchard. 2019. Trans effects on gene expression can drive omnigenic inheritance. Cell 177:1022–1034.

Lynch, M. 2020. The evolutionary scaling of cellular traits imposed by the drift barrier. Proceedings of the National Academy of Sciences 117:10435–10444.

Lynch, M. and K. Hagner. 2015. Evolutionary meandering of intermolecular interactions along the drift barrier. Proceedings of the National Academy of Sciences 112:E30–E38.

McGlothlin, J. W., M. E. Kobiela, H. V. Wright, D. L. Mahler, J. J. Kolbe, J. B. Losos, and E. D. Brodie III. 2018. Adaptive radiation along a deeply conserved genetic line of least resistance in anolis lizards. Evolution Letters 2:310–322.

McGuigan, K. 2006. Studying phenotypic evolution using multivariate quantitative genetics. Molecular ecology 15:883–896.

McGuigan, K., J. M. Collet, S. L. Allen, S. F. Chenoweth, and M. W. Blows. 2014. Pleiotropic mutations are subject to strong stabilizing selection. Genetics 197:1051–1062.

McGuigan, K., L. Rowe, and M. W. Blows. 2011. Pleiotropy, apparent stabilizing selection and uncovering fitness optima. Trends in Ecology & Evolution 26:22–29.

Melo, D. and G. Marroig. 2015. Directional selection can drive the evolution of modularity in complex traits. Proceedings of the National Academy of Sciences 112:470–475.

Nei, M. 2013. Mutation-driven evolution. OUP Oxford.

Opedal, Ø. H., W. S. Armbruster, T. F. Hansen, A. Holstad, C. Pélabon, S. Andersson, D. R. Campbell, C. M. Caruso, L. F. Delph, C. G. Eckert, et al. 2023. Evolvability and trait function predict phenotypic divergence of plant populations. Proceedings of the National Academy of Sciences 120:e2203228120.

Orr, H. A. 2000. Adaptation and the cost of complexity. Evolution 54:13–20.

Paaby, A. B. and M. V. Rockman. 2013. The many faces of pleiotropy. Trends in genetics 29:66–73.

Porto, A., H. Sebastião, S. E. Pavan, J. L. VandeBerg, G. Marroig, and J. M. Cheverud. 2015. Rate of evolutionary change in cranial morphology of the marsupial genus monodelphis is constrained by the availability of additive genetic variation. Journal of evolutionary biology 28:973–985.

Rennison, D. J. and C. L. Peichel. 2022. Pleiotropy facilitates parallel adaptation in sticklebacks. Molecular ecology 31:1476–1486.

Rolland, J., L. F. Henao-Diaz, M. Doebeli, R. Germain, L. J. Harmon, L. L. Knowles, L. H. Liow, J. E. Mank, A. Machac, S. P. Otto, et al. 2023. Conceptual and empirical bridges between micro-and macroevolution. Nature Ecology & Evolution Pages 1–13.

Schluter, D. 1996. Adaptive radiation along genetic lines of least resistance. Evolution 50:1766–1774.

Schraiber, J. G. and M. J. Landis. 2015. Sensitivity of quantitative traits to mutational effects and number of loci. Theoretical population biology 102:85–93.

Stoltzfus, A. 2021. Mutation, randomness, and evolution. Oxford University Press.

Svensson, E. I. 2022. Multivariate selection and the making and breaking of mutational pleiotropy. Evolutionary Ecology 36:807–828.

Svensson, E. I., S. J. Arnold, R. Bürger, K. Csilléry, J. Draghi, J. M. Henshaw, A. G. Jones, S. De Lisle, D. A. Marques, K. McGuigan, et al. 2021. Correlational selection in the age of genomics. Nature ecology & evolution 5:562–573.

Svensson, E. I. and D. Berger. 2019. The role of mutation bias in adaptive evolution. Trends in ecology & evolution 34:422–434.

Tenaillon, O. 2014. The utility of fisher's geometric model in evolutionary genetics. Annual review of ecology, evolution, and systematics 45:179–201.

Turelli, M. 1985. Effects of pleiotropy on predictions concerning mutation-selection balance for polygenic traits. Genetics 111:165–195.

Wagner, G. 1989. Multivariate mutation-selection balance with constrained pleiotropic effects. Genetics 122:223–234.

Wagner, G. P. 1996. Homologues, natural kinds and the evolution of modularity. American Zoologist 36:36–43.

Wagner, G. P. and L. Altenberg. 1996. Perspective: complex adaptations and the evolution of evolvability. Evolution 50:967–976.

Wagner, G. P., J. P. Kenney-Hunt, M. Pavlicev, J. R. Peck, D. Waxman, and J. M. Cheverud. 2008. Pleiotropic scaling of gene effects and the 'cost of complexity'. Nature 452:470–472.

Wagner, G. P., M. Pavlicev, and J. M. Cheverud. 2007. The road to modularity. Nature Reviews Genetics 8:921–931.

Wagner, G. P. and J. Zhang. 2011. The pleiotropic structure of the genotype–phenotype map: the evolvability of complex organisms. Nature Reviews Genetics 12:204–213.

Walsh, B. and M. W. Blows. 2009. Abundant genetic variation+ strong selection= multivariate genetic constraints: a geometric view of adaptation. Annual Review of Ecology, Evolution, and Systematics 40:41–59.

Wang, Z., B.-Y. Liao, and J. Zhang. 2010. Genomic patterns of pleiotropy and the evolution of complexity. Proceedings of the National Academy of Sciences 107:18034–18039.

Welch, J. J. and D. Waxman. 2003. Modularity and the cost of complexity. Evolution 57:1723–1734.

Zhang, X.-S. and W. G. Hill. 2005. Genetic variability under mutation selection balance. Trends in Ecology & Evolution 20:468–470.

Tables

Table 1: Definition of simulation parameters.

Parameter	Definition
z_1, z_2	Phenotypic trait 1 and trait 2
$\mathbf{M}$	Mutational variance-covariance matrix, $\mathbf{M}$-matrix
$\mathbf{M}_P$	Mutational variance-covariance matrix with only pleiotropic mutations considered
$\mathbf{G}$	Genetic variance-covariance matrix, $\mathbf{G}$-matrix
$\mathbf{R}$	Evolutionary variance-covariance matrix, $\mathbf{R}$-matrix
$\mathbb{P}$	Vector of mutational parameters, $\{U_1, \sigma_{e.1}, U_2, \sigma_{e.2}, U_P, \rho, \sigma_{p.1}, \sigma_{p.2}\}$
U_1	Rate of mutations that exclusively affect z_1
U_2	Rate of mutations that exclusively affect z_2
U_P	Rate of pleiotropic mutations that affect both z_1 and z_2
ρ	Correlation between pleiotropic mutations' effects on z_1 and z_1
$\sigma_{e.1}$	Standard deviation of effects of mutations that exclusively affect z_1
$\sigma_{e.2}$	Standard deviation of effects of mutations that exclusively affect z_2
$\sigma_{p.1}$	Standard deviation of pleiotropic mutations' effects on z_1
$\sigma_{p.2}$	Standard deviation of pleiotropic mutations' effects on z_2
C_P, C_ρ, $C_{p.1}$, $C_{p.2}$	Rescaling coefficients multiplied to U_P, ρ, $\sigma_{p.1}$, and $\sigma_{p.2}$
C_1, C_2	Rescaling coefficients multiplied to $U_1\sigma_1^2$ and $U_2\sigma_2^2$
$\mathbf{S}$	Matrix describing the fitness function
$\mathbf{H}$	Eigenvector matrix
ω	Fitness
ω_A	Ancestral fitness
s	Coefficient of selection of a mutation
N_e	Effective population size

Figures

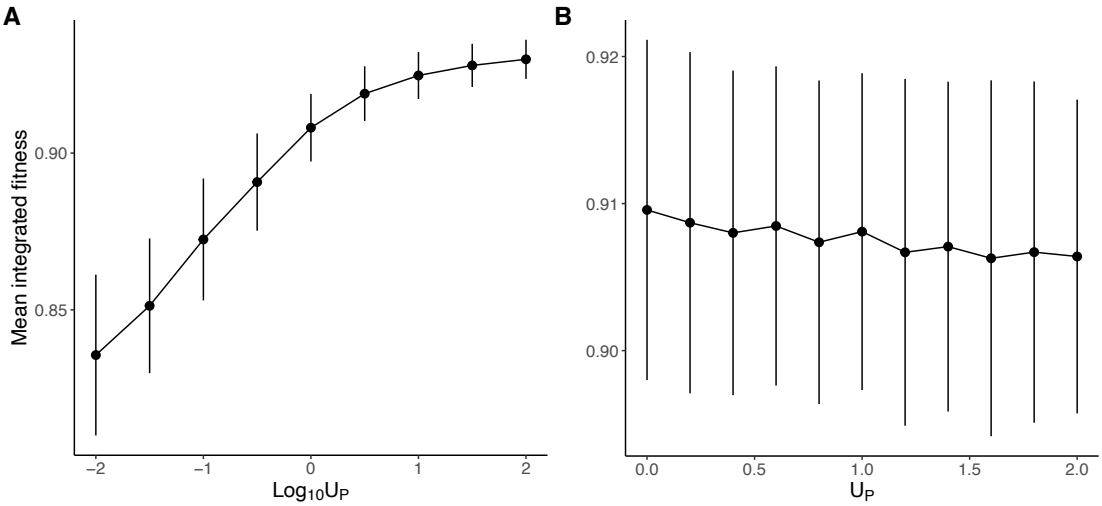

Figure 1: Relationship between rate of pleiotropic mutations (U_P) and mean integrated fitness when the mutational covariance is zero and one trait is under directional selection. Each data point represent a combination of mutational parameters that give rise to the same $\mathbf{M}$ matrix with zero covariance. (A) The effect size distribution of pleiotropic mutations varies among parameter sets (i.e., U_P, $\sigma_{p.1}$, and $\sigma_{p.2}$ vary). (B) The proportion of mutational variance attributable to pleiotropic mutations varies among parameter sets (i.e., U_1, U_2, and U_P vary). The integrated fitness is calculated based on fitness at time steps 1 to 2000. Size of each error bar is equal to twice the standard deviations of the integrated fitness.

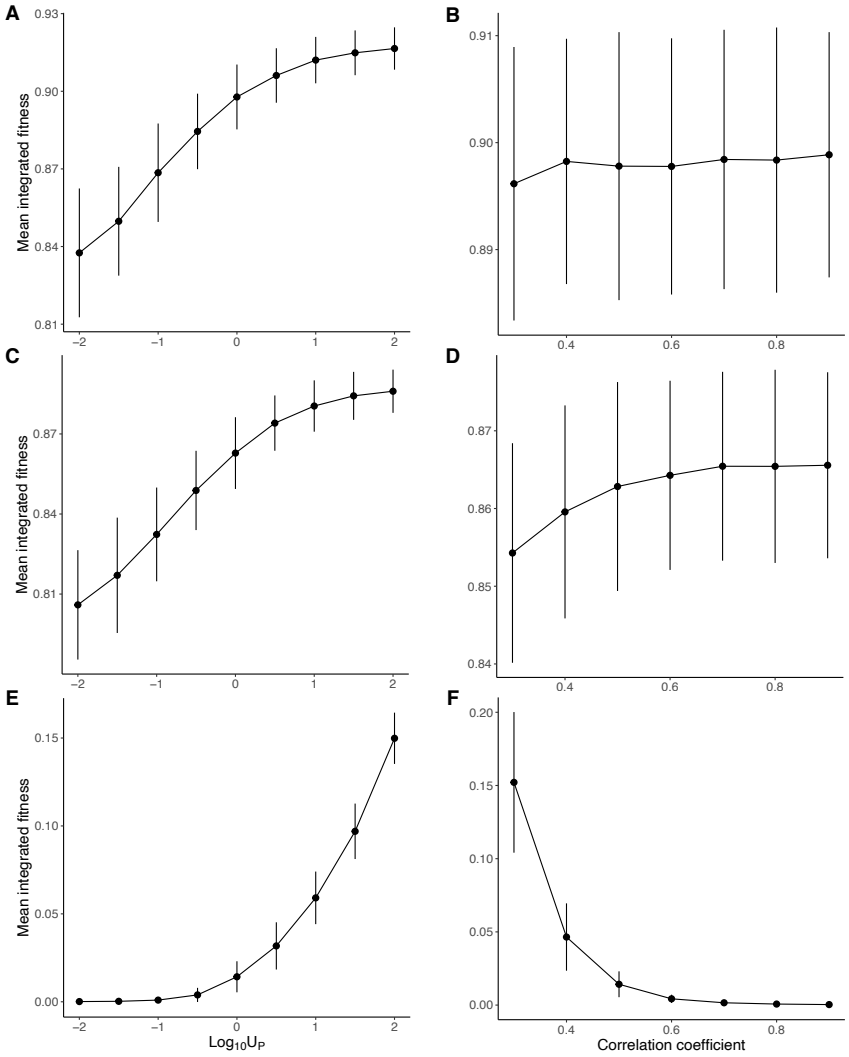

Figure 2: Relationship between rate of pleiotropic mutations (A, C, E) or correlation between pleiotropic mutations' effect on two traits (B, D, F) and mean integrated fitness when the mutational covariance is not zero. (A-B) One trait is under directional selection. (C-D) Both traits are under directional selection and the direction of selection (i.e., the line connecting the ancestral state and the optimal phenotype) is orthogonal to the first eigenvector of the $\mathbf{M}$ matrix. (E-F) Both traits are under direction selection, and both the direction of selection and the first eigenvector of the $\mathbf{S}$ matrix are orthogonal to the first eigenvector of $\mathbf{M}$. For panels (A), (C), and (E), the effect size distribution of pleiotropic mutations varies among parameter sets; for panels (B), (D), and (F), The proportion of mutational variance attributable to pleiotropic mutations varies among parameter sets. Notations are the same as those in Fig. 1.

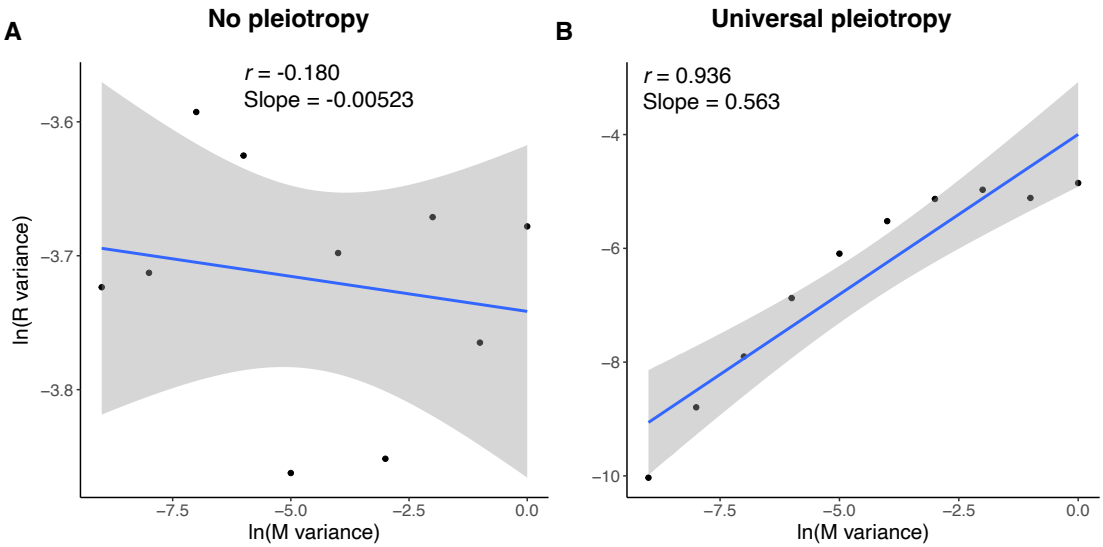

Figure 3: Correlation between log-transformed $\mathbf{M}$ and $\mathbf{R}$ variances of 10 traits when there is no pleiotropy (A) and when there is universal pleiotropy (B). The blue line in each panel is the least-squares regression line, and the gray area is the 95% confidence interval of the regression line.

Supplementary Materials

Table S1: Combinations of mutational parameters that give rise the $\mathbf{M}$ matrix with zero mutational covariance considered in the simulations. Parameter combination 1 is the "default" to start with. Combinations 2-9 vary in terms of effect size distribution of pleiotropic mutations. Combinations 10-19 vary in terms of contribution of pleiotropic mutations to mutational variances.

#	U_1	σ_1	U_2	σ_2	U_P	r	σ_a	σ_b
1	1	0.1	1	0.1	1	0	0.1	0.1
2	1	0.1	1	0.1	0.01	0	1	1
3	1	0.1	1	0.1	0.03162	0	0.5623	0.5623
4	1	0.1	1	0.1	0.1	0	0.3162	0.3162
5	1	0.1	1	0.1	0.3162	0	0.1778	0.1778
6	1	0.1	1	0.1	3.162	0	0.05623	0.05623
7	1	0.1	1	0.1	10	0	0.03162	0.03162
8	1	0.1	1	0.1	31.62	0	0.01778	0.01778
9	1	0.1	1	0.1	100	0	0.01	0.01
10	2	0.1	2	0.1	0	NA	NA	NA
11	1.8	0.1	1.8	0.1	0.2	0	0.1	0.1
12	1.6	0.1	1.6	0.1	0.4	0	0.1	0.1
13	1.4	0.1	1.4	0.1	0.6	0	0.1	0.1
14	1.2	0.1	1.2	0.1	0.8	0	0.1	0.1
15	0.8	0.1	0.8	0.1	1.2	0	0.1	0.1
16	0.6	0.1	0.6	0.1	1.4	0	0.1	0.1
17	0.4	0.1	0.4	0.1	1.6	0	0.1	0.1
18	0.2	0.1	0.2	0.1	1.8	0	0.1	0.1
19	0	NA	0	NA	2	0	0.1	0.1

Table S2: Combinations of mutational parameters that give rise the **M** matrix with a positive mutational covariance considered in the simulations. Parameter combination 1 is the "default" to start with. Combinations 2-9 vary in terms of effect size distribution of pleiotropic mutations. Combinations 10-15 vary in terms of contribution of pleiotropic mutations to mutational variances.

#	U_1	σ_1	U_2	σ_2	U_P	r	σ_a	σ_b
1	1	0.1	1	0.1	1	0.5	0.1	0.1
2	1	0.1	1	0.1	0.01	0.5	1	1
3	1	0.1	1	0.1	0.03162	0.5	0.5623	0.5623
4	1	0.1	1	0.1	0.1	0.5	0.3162	0.3162
5	1	0.1	1	0.1	0.3162	0.5	0.1778	0.1778
6	1	0.1	1	0.1	3.162	0.5	0.05623	0.05623
7	1	0.1	1	0.1	10	0.5	0.03162	0.03162
8	1	0.1	1	0.1	31.62	0.5	0.01778	0.01778
9	1	0.1	1	0.1	100	0.5	0.01	0.01
10	0.3333	0.1	0.3333	0.1	1.667	0.3	0.1	0.1
11	0.75	0.1	0.75	0.1	1.25	0.4	0.1	0.1
12	1.167	0.1	1.167	0.1	0.8333	0.6	0.1	0.1
13	1.286	0.1	1.286	0.1	0.7143	0.7	0.1	0.1
14	1.375	0.1	1.375	0.1	0.625	0.8	0.1	0.1
15	1.444	0.1	1.444	0.1	0.5555	0.9	0.1	0.1

Table S3: Phylogenetic signal, measured as Pearson's correlation between phenotypic variance among lineages and time, of traits in a 10-dimensional phenotypic space.

Trait #	**Mutational variance**	**Phylogenetic signal**	
		No pleiotropy	Universal pleiotropy
1	exp(-9)	0.773	0.990
2	exp(-9)	0.787	0.989
3	exp(-9)	0.785	0.996
4	exp(-9)	0.822	0.982
5	exp(-9)	0.715	0.979
6	exp(-9)	0.761	0.994
7	exp(-9)	0.712	0.991
8	exp(-9)	0.751	0.986
9	exp(-9)	0.689	0.978
10	1	0.677	0.986

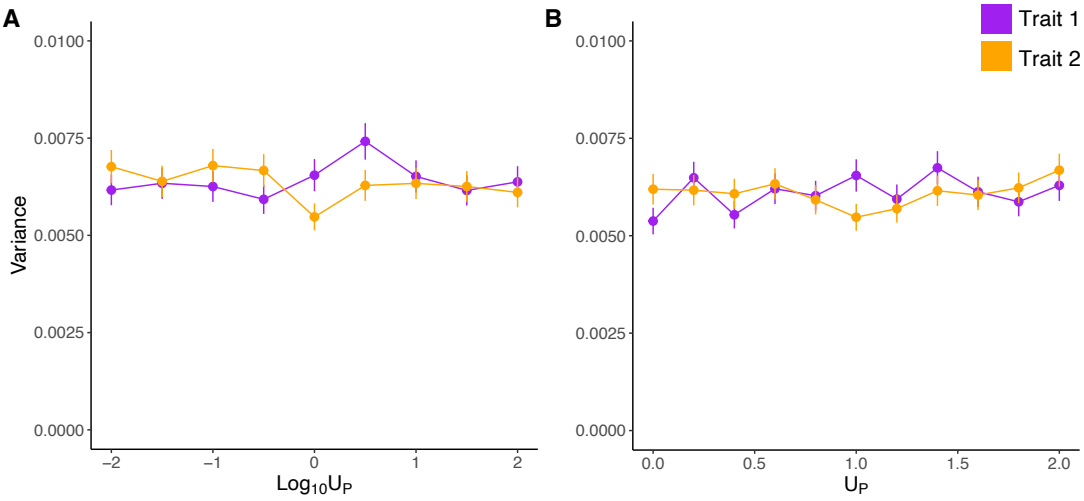

Figure S1: Relationship between rate of pleiotropic mutations (U_P) and phenotypic variance among lineages when the mutational covariance is zero and both traits are under stabilizing selection. Each data point represent a combination of mutational parameters that give rise to the same $\mathbf{M}$ matrix with zero covariance, and different colors correspond to two traits, respectively. (A) The effect size distribution of pleiotropic mutations varies among parameter sets (i.e., U_P, $\sigma_{p.1}$, and $\sigma_{p.2}$ vary). (B) The proportion of mutational variance attributable to pleiotropic mutations varies among parameter sets (i.e., U_1, U_2, and U_P vary). Size of each error bar equals twice the standard deviation of the variance ($\mathrm{SD}(V)$) and the observed variance ($\hat{V}$) is at its middle point, with the upper limit equal to $\hat{V} + \mathrm{SD}(V)$ and the lower limit equal to $\hat{V} - \mathrm{SD}(V)$.

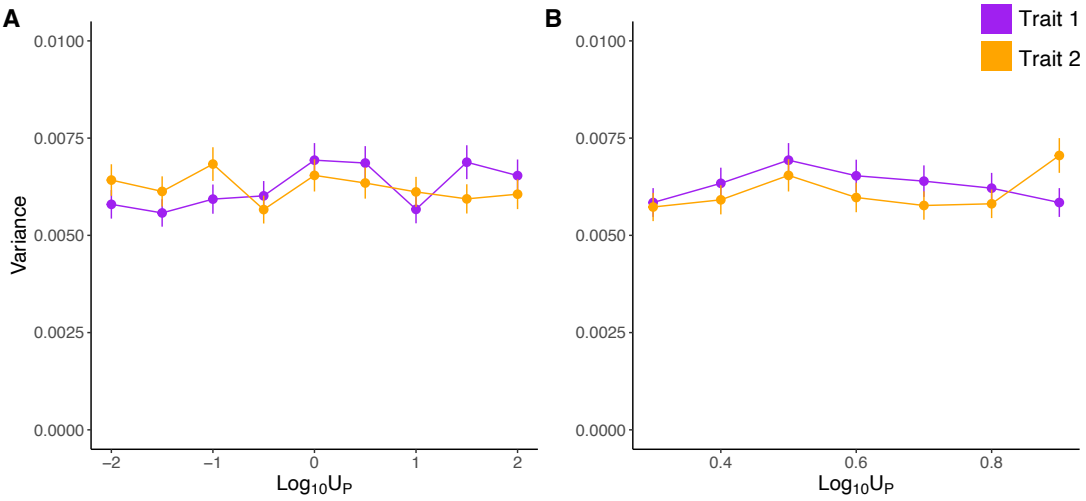

Figure S2: Relationship between rate of pleiotropic mutations (U_P) and phenotypic variance among lineages when the mutational covariance is not zero and both traits are under stabilizing selection. (A) The effect size distribution of pleiotropic mutations varies among parameter sets (i.e., U_P, $\sigma_{p.1}$, and $\sigma_{p.2}$ vary). (B) The proportion of mutational variance attributable to pleiotropic mutations varies among parameter sets (i.e., U_1, U_2, and U_P vary). Notations are the same as those used in Fig. S1.